

On the nature of Thermal Diffusion in binary Lennard-Jones liquids

Dirk Reith* and Florian Müller-Plathe

Max-Planck-Institut für Polymerforschung, Ackermannweg 10, D-55121 Mainz, Germany

(November 10, 2018)

Abstract

The aim of this study is to understand deeper the thermal diffusion transport process (Ludwig-Soret effect) at the microscopic level. For that purpose, the recently developed reverse nonequilibrium molecular dynamics method was used to calculate Soret coefficients of various systems in a systematic fashion. We studied binary Lennard-Jones (LJ) fluids near the triple point (of one of the components) in which we separately changed the ratio of one of the LJ parameters mass, atomic diameter and interaction strength while keeping all other parameters fixed and identical. We observed that the magnitude of the Soret coefficient depends on all three ratios. Concerning its sign we found that heavier species, smaller species and species with higher interaction strengths tend to accumulate in the cold region whereas the other ones (lighter, bigger or weaker bound) migrate to the hot region of our simulation cell. Additionally, the superposition of the influence of the various parameters was investigated as well as more realistic mixtures. We found that in the experimentally relevant parameter range the contributions are nearly additive and that the mass ratio often is the dominating factor.

*corresponding author

I. INTRODUCTION

Transport processes play an important role in the understanding of the properties of liquid mixtures. Thermal diffusion (the Ludwig-Soret effect) is one of these intriguing processes. It characterizes the flux of matter in response to a gradient in temperature and has already been studied for almost 150 years: The migration of atoms and molecules as a consequence of a temperature gradient was first reported by Ludwig¹ when studying sodium-sulfate solutions in 1856. Later, in 1879, Soret² observed the same effect in other electrolyte solutions. In the case of gases, it was predicted independently by Enskog³ and by Chapman⁴, and later confirmed by the experiments of Chapman and Dootson⁵. Further, several small organic molecule or polymer mixtures have been investigated by various experimental methods such as thermo-gravitational columns (e.g. Clusius and Dickel⁶), thermal field flow fractionation (e.g. Giddings⁷) or most recently by thermal diffusion forced Rayleigh scattering (Köhler⁸). There are numerous examples for the technological significance of thermal diffusion, e.g. presented by Kincaid, Ratkje and Hafskjøld^{9,10}. However, there is still no satisfactory theory to explain the effect. “It is the only hydrodynamic transport mechanism that lacks a simple physical explanation.”⁹. But the situation is even worse: One cannot even approximately predict the transport coefficients of closely related systems. The size of the Ludwig-Soret effect differs e.g. for equimolar mixtures of benzene-chlorobenzene and benzene-nitrobenzene roughly by a factor of 10¹¹. Additionally, the experimental data base is rather small and partly inconsistent⁸. One reason for this is probably that thermally driven flows of matter are minor effects and thus several orders of magnitude smaller than concentration driven flows.

In multi-component systems, couplings between the different types of transport are, on a fundamental level, described by Onsager’s linear relationships¹²:

$$\begin{aligned}\vec{J}_k &= \sum_{j=1}^N L_{kj} \vec{X}_j + L_{kq} \vec{X}_q & k = 1, \dots, N \\ \vec{J}_q &= \sum_{j=1}^N L_{qj} \vec{X}_j + L_{qq} \vec{X}_q\end{aligned}\tag{1.1}$$

with \vec{J}_k being the flux of component k in $\text{gcm}^{-2}\text{s}^{-1}$ with respect to the center of mass of the system and \vec{J}_q being the heat flux in $\text{Jcm}^{-2}\text{s}^{-1}$. The \vec{X}_α are thermodynamic forces, specifically for a binary mixture $\vec{X}_q = -\frac{\vec{\nabla}T}{T}$ and $\vec{X}_j = -\vec{\nabla}_T(\mu_1 - \mu_2)$. (The subscript T denotes that the gradient has to be taken under isothermal conditions.) The $L_{\alpha\beta}$ are the Onsager coefficients with $\alpha = (k, q)$ and N is number of species in the mixture. Note that this representation assumes $\vec{J} \parallel \vec{X}$, otherwise each $L_{\alpha\beta}$ has to be a 3×3 tensor. The assumption of linear response holds for many transport processes through

condensed media. In this picture, thermal diffusion is characterized by the matrix coefficient L_{kq} .

Although equations 1.1 have been known for several decades, there is yet no deeper insight into the microscopic mechanisms of the *coupling* of heat and mass transport. Liquid mixtures are often difficult to understand by analytical theories. Performing computer simulations, in contrast, is a way to look easily at the microscopic properties of a liquid system. The most promising results to understand thermal diffusion seem to come from molecular dynamics (MD) simulations. Several MD techniques have been developed in order to study the Ludwig-Soret effect. The early algorithms suffered from conceptual as well as practical problems: firstly, of how to define and compute the heat flow or the heat of transfer accurately in the microscopic picture and, secondly, from the large perturbation fields that were necessary to observe thermal diffusion^{13–17}). Hafskjøld et al.¹⁸ were the first to develop an algorithm that side-steps these problems. In fact, their methods are similar in spirit to ours. They define microscopic fluxes in an unambiguous way. However, they mostly investigated dilute gas mixtures⁹ or interfacial systems^{18–20} so far. To our knowledge, there is no systematic study of thermal diffusion in the high density liquid regime up to present.

In this contribution, we study both qualitative and quantitative aspects of the Ludwig-Soret effect. This is done by performing reverse non-equilibrium molecular dynamics (RNEMD) computer simulations for binary Lennard-Jones (LJ) systems. We investigate the influence of systematic variations of the physical parameters (mass m , atomic diameter σ and interaction strength ε) of our model system: By changing one parameter ratio (e.g. m_1/m_2) while keeping all other parameters fixed and identical, we are able to observe exactly how the Ludwig-Soret effect depends on every one of them separately. We exploit the advantage of better control of the system variables in computer simulation over experiment to better understand thermal diffusion. We discuss our simulation results in the framework of linear irreversible thermodynamics. Moreover, we establish empirical rules for the influence of differences in the individual molecular parameters on the Ludwig-Soret effect and finally investigate to which extent they are additive.

II. THEORY

Linear Irreversible Thermodynamics

In order to define proper quantities in the theory of linear irreversible thermodynamics, the assumption of local equilibrium is essential. It enables us to apply the well-known equilibrium machinery to local volume elements of a perturbed system by defining intensive quantities derived from the extensive equilibrium quantities²¹. The entropy source strength s given in $\frac{J}{s \cdot K \cdot cm^3}$ is the

fundamental quantity of this theory. Due to Onsager's variational principle¹², $s \geq 0$ has to be minimized. The non-equilibrium steady state is the one in which the least amount of total entropy is produced:

$$\int_V s(\vec{r}, t) dV \longrightarrow \min! \quad (2.1)$$

It is also the state in which heat is most efficiently conducted through the system. Using a local form of the Gibbs equation in connection with the continuity equation for the entropy (for details, see e.g. ²²) leads to the following equation for s in a binary system with coupled flux of heat and matter:

$$s(\vec{r}, t) = - \left[\vec{J}_q(\vec{r}, t) \cdot \vec{\nabla} T(\vec{r}, t) \right] \frac{1}{T(\vec{r}, t)^2} - \left[\vec{J}_1 \cdot \vec{\nabla}_T \mu(\vec{r}, t) \right] \frac{1}{T(\vec{r}, t)} \quad (2.2)$$

with \vec{J}_1 being the mass flux of species 1 in $\frac{g}{cm^2 s}$ with respect to the center of mass of the system, \vec{J}_q the heat flux in $\frac{J}{cm^2 s}$, $\mu = \mu_1 - \mu_2$ the effective chemical potential in $\frac{J}{g}$ and T the temperature in K . The right hand side of equation 2.2 is the sum of products of the fluxes (of heat and matter), thermodynamic forces (the gradients) and of 'thermodynamic factors' $\frac{1}{T^2}$ and $\frac{1}{T}$, respectively. The latter provide for the correct dimensions. In this article, we consider the time-independent steady state in which the matter flux has died out and a constant temperature gradient is the only origin for the entropy source strength:

$$s(\vec{r})_{\vec{J}_1=0} = - \left[\vec{J}_q(\vec{r}) \cdot \vec{\nabla} T \right] \frac{1}{T(\vec{r})^2}. \quad (2.3)$$

Combining this with Fourier's law for heat conduction we get:

$$s(\vec{r})_{\vec{J}_1=0} = -\lambda_{av} \left(\frac{\vec{\nabla} T}{T(\vec{r})} \right)^2. \quad (2.4)$$

The thermal conductivity depends on density, temperature and concentration of the mixture, which may vary over the system. Still, we assume that the perturbation and, hence, the variation in these quantities is small enough, so it is sensible to use an average thermal conductivity λ_{av} . The magnitude of the temperature gradient $\vec{\nabla} T$ is the decisive quantity of the entropy source strength in our binary system. Note finally, that the local entropy production increases towards the cold region of the system as $1/T(\vec{r})^2$.

Phenomenological Transport Coefficients

Equations 1.1 give the impression of a universal, clean and symmetric ($L_{\alpha\beta} = L_{\beta\alpha}$) theory. Unfortunately, they have the disadvantage that the quantities of interest (i.e. the Onsager coefficients and the thermodynamic forces) are

related to but not identical with experimentally measurable transport coefficients and fields. The relations between them and the Onsager coefficients $L_{\alpha\beta}$ are well known (cf. e.g. ^{23,22}). In their analysis, RNEMD simulations are akin to experiment²⁴, so in the following we will concentrate on the relevant experimental transport coefficients: the self diffusion coefficients D_k ($k = 1, 2$) (dimension cm^2/s) and the Soret coefficient S_T (dimension $1/K$). The former are calculated in our simulations via the Einstein route:

$$D_k = \frac{1}{6} \frac{d}{dt} \left\langle \left| \vec{r}_j^{(k)}(t) - \vec{r}_j^{(k)}(0) \right|^2 \right\rangle. \quad (2.5)$$

Averaging is performed over time origins as well as over all particles j of type k . Since we empirically found that the D_k calculated out of RNEMD simulations are (within statistical uncertainty) identical with equilibrium data (as we checked for some systems), we skipped further equilibrium runs to save resources and use the RNEMD data. The Soret coefficient is defined as $S_T = D_T/D_{12}$ and has the physical meaning of the relative strength between thermally induced diffusion (characterized by the thermal diffusion coefficient D_T) and concentration-driven, Fickian diffusion (characterized by the mutual diffusion coefficient D_{12}). Phenomenologically, thermal diffusion is often expressed as

$$J_1 = -D_{12}\rho \left[\left(\frac{\partial w_1}{\partial z} \right) + S_T w_1 (1 - w_1) \left(\frac{\partial T}{\partial z} \right) \right]. \quad (2.6)$$

Here, we are assuming field (temperature gradient) and fluxes (energy and matter) in z direction. J_1 is the flux of species 1, ρ the average mass density (assuming that the temperature gradient and the resulting density gradient are small) and $w_1 = x_1 m_1 / (x_1 m_1 + x_2 m_2)$ the weight fraction of species 1 (x_k denotes the mole fraction of species k). Equation 2.6 appears to be similar to Onsager's description (Equations 1.1). Note, however, that the gradient of the chemical potential has been replaced by the experimentally more accessible and technologically more relevant weight fraction gradient. If the system is continuously subjected to a temperature gradient, it will be driven to a non-equilibrium steady state: energy (heat) is then constantly flowing through it while the mass flux has stopped ($J_1 = 0$) and a constant concentration (or weight fraction) gradient has been established. Equation 2.6 can then be simplified and S_T , after application of the chain rule, be obtained from the temperature and molar fraction gradients in the system:

$$S_T = -\frac{1}{w_1(1-w_1)} \left(\frac{\partial w_1}{\partial z} \right) \left(\frac{\partial T}{\partial z} \right)^{-1} = -\frac{1}{x_1(1-x_1)} \left(\frac{\partial x_1}{\partial z} \right) \left(\frac{\partial T}{\partial z} \right)^{-1}. \quad (2.7)$$

In the special case of equimolar mixtures ($x_1 = x_2 = 0.5$), equation 2.7 reduces further to

$$S_T = -4 \left(\frac{\partial x_1}{\partial z} \right) \left(\frac{\partial T}{\partial z} \right)^{-1} \quad (2.8)$$

The gradients appearing in equation 2.8 can be calculated directly in our RNEMD simulations, making the analysis of the simulation data swift and easy. In particular, S_T can be calculated without previous evaluation of D_T and D_{12} . Throughout this work, positive values of S_T signify, that species 1 tends to accumulate in the *cold* regions of the simulation box.

III. COMPUTATIONAL DETAILS

Model System and Simulation Details

All simulations are performed with 1500 Lennard-Jones (LJ) atoms²⁵ with cutoff distance $r_c = 2.5\sigma_1$, $\sigma_1 \geq \sigma_2$. The potential is defined as:

$$U_{LJ}(r) = 4\epsilon \left[\left(\frac{\sigma}{r}\right)^{12} - \left(\frac{\sigma}{r}\right)^6 \right]. \quad (3.1)$$

We investigate equimolar mixtures of two species only. Consequently, our model system has six physical parameters: atomic masses m_k ($k = 1, 2$), atomic diameters (in form of σ_k) and the interaction strengths (in form of ϵ_k) of our two model species. For the interaction between unlike particles, the Lorentz-Berthelot mixing rules²⁵ are applied. No corrections to the interaction parameters due to excess functions (e.g. molar volume and enthalpy) are considered, although that can be done and might be useful in case of more realistic simulations. The orthorhombic periodic simulation cell is of size $(L^* \times L^* \times 3L^*)$, with L^* being roughly 8–13. The asterisk indicates Lennard-Jones reduced units²⁵, using LJ-Argon values as reference values (Table I). The volume is held constant during the simulation. Our simulations are performed in the dense liquid state, i.e. $\bar{\rho}^* = 0.8 - 0.85$ and $\bar{T}^* = 0.75 - 0.85$ (Table I), which is close to the triple point of species 2. The average temperature \bar{T}^* is maintained at its value by the weak-coupling scheme of Berendsen²⁶ with a coupling time of $t_{coup}^* = 4.66$. We do so to prevent long-time drifts which might occur due to limited precision of the discrete, stepwise solution of the equations of motion. They are integrated using the velocity-Verlet algorithm in connection with a multiple-time-step scheme²⁷ for the force calculations. Long-range forces ($r > 1.7\sigma_m$ with $\sigma_m = \max\{\sigma_1, \sigma_2\}$) are evaluated only every 4 time steps $\Delta t^* = 4.66 \cdot 10^{-3}$, the switching range is $0.1\sigma_m$. Our simulations are performed with run lengths of $3 \cdot 10^6 - 10 \cdot 10^6$ steps. Shorter preparatory-runs of $0.8 \cdot 10^6 - 1.5 \cdot 10^6$ steps are made to establish the non-equilibrium steady state. The runs have to be that long because the fluctuations in the mole fraction profile are relatively large and thermal diffusion is a weak effect compared to other transport properties. Positions and velocities are written out every 500–3000 steps, local temperature and concentration in the slabs (see below) every 50–100 steps for calculation of the relevant gradients.

The RNEMD algorithm

The RNEMD method reverses the usual cause-and-effect picture of non equilibrium simulations. For the study of thermal diffusion the “effect”, the heat flux, is imposed on the system whereas the “cause”, the temperature gradient is obtained from the simulation: We divide the simulation cell into $N_s = 20$ slabs perpendicular to the z -direction (Fig. 1). The slabs are chosen to be equally thick, i.e. to have identical volumes, and large enough so that reasonable statistics can be expected: each slab contains 75 particles on average. A flow of heat \tilde{J}_q is artificially maintained by exchanging velocities of suitably selected particles : Slab 0 is defined as the ‘cool’ slab and slab $N_s/2$ as the ‘hot’ slab. Every N_{exch} steps, we search through all atoms of the cold slab and determine the hottest ones of both species. In the hot slab, we proceed conversely and determine the coldest atoms of both species. Then we exchange the velocities of the so determined atoms of the same species. We were always able to find at least one particle in the cold slab that is hotter than the coldest particle of the hot slab, since the Maxwell-Boltzmann distribution of atomic kinetic energies is very broad compared to the temperature difference of the two slabs. The exchange period has to be adjusted such that the perturbation is weak enough for linear response to hold (typically: $N_{exch} = 50 - 200$ steps). This leads to a temperature variation of $2(T_{hot}^* - T_{cold}^*)/(T_{hot}^* + T_{cold}^*) \approx 0.1 - 0.15$. It was shown^{22,24,28} that for temperature differences of up to half the average temperature linear response is still approximately fulfilled. The unphysical velocity exchange leads to a *physical* flux of heat in the opposite direction through the intervening slabs. As the response is linear, the procedure causes linear profiles of temperature, overall density and concentration (Fig. 2). At steady state, physical and unphysical heat flux have the same magnitude because of energy conservation. Thus, cf. equation 2.4, the temperature gradient will be minimal. To avoid a possible breakdown of the local equilibrium due to the unphysical energy transfer in the thermostatted slabs, these are excluded from gradient calculations. General properties and details of the RNEMD technique as well as how to compute other transport coefficients with it have been published elsewhere^{24,28,29}.

IV. RESULTS AND DISCUSSION

Data Comparison with other Work

Since the Ar-Kr LJ-system was mostly investigated by MD computer simulations in the past, we made a consistency check of our results with such a system. Table II compares our own results with data obtained by several other groups, all using identical LJ-parameters for Ar and Kr, respectively

(Table III). For the self diffusion coefficients, the agreement is excellent. The situation is different concerning the Soret coefficient. It can be seen, that although the signs for S_T are identical and all values lie close to each other, they do not agree with each other within the statistical uncertainty. However, comparison with the older results is somewhat difficult since system sizes were much smaller (128 or 256 particles). Moreover, we found in our simulations that the value of S_T is strongly influenced by the specific state point at which the simulation was run. Minor shifts in the density were e.g. sufficient to change the value of S_T by more than 30% (Table II). Vogelsang and Hoheisel reported¹⁶, that their values are systematically too low due to an inaccurate determination of the partial enthalpies. Extrapolation to zero field strength (MacGowan and Evans^{13,14}, Paolini and Cicotti¹⁵) or zero temperature gradient (as in our case) are also sources of error. Figure 3 shows that in our simulations the Soret coefficients can be well extrapolated to zero field. The two outermost points deviate from the extrapolation line for two different reasons. At low temperature gradients (left) there is too much statistical uncertainty in the concentration gradient. At high gradient (right) the linear response breaks down because of the too large perturbation. Additionally, the temperature of the cool region lies then below the freezing temperature.

Systematic Variations of Parameters

As long as we change only one parameter ratio at a time, the problem is symmetric in species identity, i.e. it is sufficient to consider ratios larger than 1.0. We define species 2 as reference species and identify it with LJ-Argon: $m_2 = 39.95$ amu, $\sigma_2 = 0.3405$ nm and $\varepsilon_2 = 1.0$ kJ/mol. When changing the mass ratio while keeping all other parameters fixed and identical, the positive sign of S_T indicates that the heavier species 1 prefers the cold side of the simulation box whereas the lighter species 2 favors the hot side (Fig. 4). Moreover, S_T rises monotonically for the whole mass ratio range. As a side result we found that the behaviour of the self diffusion coefficients could be very well fitted by power laws: $D_1 \propto (m_1/m_2)^{-0.342}$ and $D_2 \propto (m_1/m_2)^{-0.252}$, which is very close to exponents $-\frac{1}{3}$ and $-\frac{1}{4}$. They are also similar to those first found by Bearman and Jolly in simulations of Ar-Kr mixtures (-0.3 and -0.2 , respectively)³⁰. For the interaction parameter ε it can be seen that S_T is positive for $\varepsilon_1 > \varepsilon_2$ (Fig. 5), i.e. species with deeper potential wells prefer the cold side of the simulation box while the more weakly bound species accumulate on the hot side. The effect of mass and interaction strength variations is intuitively understandable since both times, the species with the lower mobility (i.e. lower self diffusion coefficient, cf. Fig. 4, 5) favors the cold area.

For the atomic diameter parameter σ , in contrast, we find that S_T is negative for $\sigma_1 > \sigma_2$, i.e. smaller particles prefer the cold side of the simulation box although their mobility is higher compared to the bigger species (Fig. 6).

Furthermore, a monotonic behavior was only found for $\sigma_1/\sigma_2 < 1.25$ (which would already be large for realistic mixtures). A pressure effect can here be ruled out as the pressure did not vary more than 5%. For higher ratios, the S_T data points do not show a monotonic behaviour any more. Here, we also found a large disparity of the two self diffusion coefficients. Specifically, the bigger species becomes increasingly immobile compared to the smaller species and the absolute number of bigger particles per slab is nearly constant (Fig. 7). That indicates that a regime is reached in which the mobility of the larger particles is massively hindered by their own space-filling arrangement in the box. Therefore, the large particles can no longer exhibit a density gradient. As a consequence, the small species remains the only one capable to accumulate in the cold region: It is done for entropic reasons (the cooler a region, the higher the overall density). Now the question arises if the trend 'the bigger the species, the more it tends to accumulate in the hot region' still holds if both species can move around unhindered. Therefore, a run with lower density and higher temperature ($\sigma_1/\sigma_2 = 1.4$, $\rho^* = 0.6$, $T^* = 1.15$) was performed. The bigger species then builds up a concentration gradient and accumulates at the hot side with $S_T = -6.1 \pm 0.6$, confirming the trend observed for atomic diameter ratios. However, the high ratio regime is artificial and the above explanation not applicable in the realistic area of $\sigma_1/\sigma_2 < 1.25$. There, another argument seems to be more appropriate: If we combine the LJ parameters σ and ε into the variable $e = \frac{\varepsilon}{\sigma^3}$ we obtain a measure for the stored energy per volume, a potential or cohesive energy density. The Soret coefficient varies linearly with the ratio e_1/e_2 (Fig. 8). The species with higher cohesive energy density accumulates in the cold region of the system.

Realistic systems and superposition of different contributions to the Soret coefficient

We also investigated how more complicated mixtures (species differing in all parameters) behave under the influence of a temperature gradient. Thus, we can check if the parameters contribute more or less independently to the Soret coefficient and if one of them is dominating. The investigated systems comprised all possible liquid binary mixtures of Ar , Kr , Xe and CH_4 (Table V), representing species with strongly deviating parameters. The following empirical laws were obtained by low order fits of the independent parameter variations (Table IV):

$$S_T[10^{-3}/K] = -0.7 \cdot \left(\frac{m_1}{m_2} \right)^2 + 9.5 \cdot \left(\frac{m_1}{m_2} \right) - 8.8 \quad \text{for } m_1/m_2 \leq 8.0 \quad (4.1)$$

$$S_T[10^{-3}/K] = 67.4 \cdot \left(\frac{\sigma_1}{\sigma_2} \right)^2 - 179.3 \cdot \left(\frac{\sigma_1}{\sigma_2} \right) + 111.9 \quad \text{for } \sigma_1/\sigma_2 \leq 1.25 \quad (4.2)$$

$$S_T[10^{-3}/K] = 4.4 \cdot \left(\frac{\varepsilon_1}{\varepsilon_2} \right)^2 + 3.5 \cdot \left(\frac{\varepsilon_1}{\varepsilon_2} \right) - 7.9 \quad \text{for } \varepsilon_1/\varepsilon_2 \leq 1.75 \quad (4.3)$$

Using the additivity of the three contributions, we predicted the Soret coefficients of the realistic systems and compared them, using Eqns. 4.1, 4.2 and 4.3, with the simulated values (Fig. 9). The agreement is excellent: The sign of S_T is correct for all cases and the relative deviation is below 30% for all realistic mixtures. The results show also clearly that increasing Soret coefficients are mainly correlated with increasing mass ratios (Fig. 9). That is because in realistic systems (of unlike noble gases), the mass difference between the two species is usually much larger than the deviations in their effective diameter or interaction strength. Additionally, the effects of σ and ε tend to cancel out each other, since mostly, the bigger atom is also the one with the deeper potential well. For this reason it is possible to combine the last two equations (4.2 and 4.3) into a single one which involves the cohesive energy densities. That is done by fitting a straight line to the composed data shown in Fig. 8:

$$S_T[10^{-3}/K] = 14.8 \cdot \left(\frac{e_1}{e_2} \right) - 14.8 \quad (4.4)$$

As it can be seen in Table V, the accuracy of the prediction using Eqns. 4.1 and 4.4 is the same compared to Eqns. 4.1, 4.2 and 4.3 for most data points. Only in the case of the Xe-Ar mixture, the predicted values differ significantly. Here, the latter prediction is much lower than the first one. That is most probable because the individual parameter ratios are large (and, hence, tend to be more inaccurate) while, due to compensation effects, the composed ratio does not differ much from unity compared to the other mixtures. To check if the empirical laws are applicable to experimental data, we compared the predicted results for equimolar mixtures of benzene-chlorobenzene and benzene-nitrobenzene (mentioned in the introduction) to the experimental values. The sign as well as the order of magnitude of S_T could be reproduced: For benzene-chlorobenzene, $S_T(\text{pred}) = -5.0 \cdot 10^{-3}$ (exp.: $-1.1 \cdot 10^{-3}$) and for benzene-nitrobenzene $S_T(\text{pred}) = -12.6 \cdot 10^{-3}$ (exp.: $-11.0 \cdot 10^{-3}$). In view of the simplicity of the model, we consider this as an excellent result which motivates us to continue work in this direction.

V. CONCLUSIONS

We investigated with computer simulations thermal diffusion processes in simple two-component Lennard-Jones model liquids out of equilibrium. We observed that for dense liquid mixtures, the size of the Ludwig-Soret effect, depends on the ratios of all three model parameters: the mass, the atomic diameter and the interaction strength. However, the combination of the two latter into a single parameter $e = \frac{\varepsilon}{\sigma^3}$, the potential energy density of a species, seems to be especially appropriate to explain the sign of the Ludwig-Soret effect.

Parts of our results are in line with earlier investigations, especially by Vo-gelsang and Hoheisel et al.^{31,32} and Hafskjøld et al.^{23,9}, while others are com-

pletely new. For isotopic systems, the lighter species can transport a higher amount of heat through the system if it accumulates in the hot region. Moreover, the possibility to superpose the influence of the various parameters was investigated on more realistic mixtures of LJ noble gases. For most of these systems, the mass ratio is the dominating factor that determines sign and value of S_T . This trend is for realistic mixtures augmented by the fact, that the effects of σ and ε tend to cancel out each other, since bigger species often also are the ones with the deeper potential depth. Further investigations will compare our simulation results with experimental data.

ACKNOWLEDGEMENTS

We gratefully acknowledge Burkhard Dünweg, Simone Wiegand and Werner Köhler for fruitful discussions.

List of Tables

I	Reduced units for physical quantities. LJ-Argon was taken to be the reference system (Table III). The mixed quantities σ_{12} and ε_{12} are derived by the Lorentz-Berthelot rules. For density and temperature they were used to conserve the state point in the phase diagram of the mixed system.	13
II	Comparison of calculated values for the Soret and self diffusion coefficients of a Lennard-Jones Ar-Kr binary mixture.	14
III	Lennard-Jones parameters for the atoms and molecules of this study. Molecules are treated as single Lennard-Jones atoms.	15
IV	Thermal Diffusion data: Separate variation of every species 1 parameter at the state point $\bar{T}^* = 0.85$, $\bar{\rho}^* = 0.81$. Species 2 corresponds to Lennard-Jones Argon. The error is estimated by linear regression (in case of S_T of the temperature and mole fraction profiles). For the self diffusion coefficients, the error is generally $\pm 2\%$. . .	16
V	Soret coefficients for several simple atomic systems at the state point $\bar{T}^* = 0.85$, $\bar{\rho}^* = 0.81$. The run length was $4.0 \cdot 10^6$ steps. Additionally, the data for two isotopic systems is presented. A comparison indicates, that S_T is chiefly governed by the mass ratio. The error is estimated by error propagation from the errors of the slopes of temperature and mole fraction profiles as obtained in the linear regression. . .	17

TABLES

Quantity	Reduced units
Mass	$m_j^* = \frac{m_j}{m_{Ar}}$
Length	$r^* = \frac{r}{\sigma_{Ar}}$
Energy	$E^* = \frac{E}{\varepsilon_{Ar}}$
Time	$t^* = \frac{t}{\sigma_{Ar}} \sqrt{\frac{\varepsilon_{Ar}}{m_{Ar}}}$
Diffusion coefficient	$D^* = \frac{D}{\sigma_{Ar}} \sqrt{\frac{m_{Ar}}{\varepsilon_{Ar}}}$
Soret coefficient	$S_T^* = S_T \frac{\varepsilon_{Ar}}{k_B}$
Pressure	$p^* = p \frac{\sigma_{Ar}^3}{\varepsilon_{Ar}}$
Density	$\rho^* = \frac{N\sigma_{12}^3}{V}$
Temperature	$T^* = \frac{k_B T}{\varepsilon_{12}}$

TABLE I. Reduced units for physical quantities. LJ-Argon was taken to be the reference system (Table III). The mixed quantities σ_{12} and ε_{12} are derived by the Lorentz-Berthelot rules. For density and temperature they were used to conserve the state point in the phase diagram of the mixed system.

Ref.	Method ¹	Number of atoms	ρ^*	T^*	S_T [$10^{-3} K^{-1}$]	D_{Ar} [$10^{-5} cm^2 s^{-1}$]	D_{Kr} [$10^{-5} cm^2 s^{-1}$]
ME ²	NEMD	108,256	0.7902	0.805	11.3		
PC ³	NEMD	108,256	0.7902	0.824	16.2 ± 2.0		
VH ⁴	EMD	108,256	0.803 0.79	0.81 0.80	9.1 ± 2.0	2.97 ± 0.08	2.60 ± 0.08
SH ⁵	EMD	256	0.79	0.81		2.97 ± 0.08	2.44 ± 0.08
this work	NEMD	1500	0.797	0.805	10.5 ± 1.3	2.98 ± 0.05	2.48 ± 0.05
this work	NEMD	1500	0.81	0.85	14.4 ± 1.2	2.97 ± 0.05	2.47 ± 0.05

TABLE II. Comparison of calculated values for the Soret and self diffusion coefficients of a Lennard-Jones Ar-Kr binary mixture.

¹ EMD: Equilibrium Molecular Dynamics, NEMD: Non-Equilibrium Molecular Dynamics

² MacGowan and Evans¹³

³ Paolini and Cicotti¹⁵

⁴ Vogelsang and Hoheisel¹⁶

⁵ Schön and Hoheisel³³

Atom species	$m[amu] = m^*$	$\sigma[nm] = \sigma^*$	$\varepsilon[kJ/mol] = \varepsilon^*$
Ar	39.95=1.00	0.3405=1.00	1.00=1.00
Kr	83.80=2.10	0.3633=1.07	1.39=1.39
Xe	131.29=3.29	0.3975=1.17	1.72=1.72
CH_4	16.04=0.40	0.3740=1.10	1.27=1.27

TABLE III. Lennard-Jones parameters for the atoms and molecules of this study. Molecules are treated as single Lennard-Jones atoms.

m_1/m_2	σ_1/σ_2	$\varepsilon_1/\varepsilon_2$	S_T [$10^{-3}K^{-1}$]	D_1 [$10^{-5}cm^2s^{-1}$]	D_2 [$10^{-5}cm^2s^{-1}$]	p [10^7Pa]
1.2	1.0	1.0	1.4 ± 0.2	2.96	2.96	4.6 ± 0.4
1.5	1.0	1.0	5.0 ± 0.5	2.79	2.82	4.6 ± 0.3
2.0	1.0	1.0	8.9 ± 0.7	2.63	2.69	4.7 ± 0.3
3.0	1.0	1.0	15.7 ± 0.5	2.30	2.37	4.7 ± 0.3
4.0	1.0	1.0	19.4 ± 0.9	2.09	2.31	4.6 ± 0.3
6.0	1.0	1.0	23.4 ± 0.6	1.69	1.96	4.6 ± 0.4
8.0	1.0	1.0	24.6 ± 0.8	1.51	1.79	4.6 ± 0.4
1.0	1.0	1.1	1.2 ± 0.3	2.99	3.00	4.9 ± 0.4
1.0	1.0	1.2	2.7 ± 0.4	3.03	3.06	5.0 ± 0.4
1.0	1.0	1.3	4.1 ± 0.5	3.10	3.23	5.2 ± 0.4
1.0	1.0	1.4	5.5 ± 0.8	3.12	3.34	5.3 ± 0.4
1.0	1.0	1.5	7.3 ± 0.7	3.14	3.40	5.3 ± 0.4
1.0	1.0	1.75	11.6 ± 0.6	3.17	3.53	5.5 ± 0.4
1.0	1.0	2.0	21.0 ± 0.4	3.15	3.71	5.8 ± 0.5
1.0	1.0	2.25	30.7 ± 0.9	3.13	3.87	5.9 ± 0.6
1.0	1.0	2.5	41.4 ± 2.6	3.05	4.00	6.0 ± 0.7
1.0	1.05	1.0	-2.6 ± 0.5	2.90	3.11	4.1 ± 0.3
1.0	1.1	1.0	-3.6 ± 0.5	2.89	3.18	3.9 ± 0.3
1.0	1.15	1.0	-5.4 ± 0.5	2.78	3.21	3.9 ± 0.3
1.0	1.2	1.0	-6.1 ± 0.5	2.62	3.27	3.8 ± 0.2
1.0	1.25	1.0	-7.1 ± 0.5	2.56	3.31	3.8 ± 0.2
1.0	1.3	1.0	-6.1 ± 0.6	2.46	3.29	4.0 ± 0.2
1.0	1.35	1.0	-5.7 ± 0.6	2.37	3.17	4.2 ± 0.2
1.0	1.4	1.0	-7.0 ± 0.5	2.09	3.16	4.4 ± 0.2
1.0	1.5	1.0	-5.2 ± 0.5	1.72	3.04	5.0 ± 0.2
1.0	1.7	1.0	-8.4 ± 0.7	1.14	2.45	6.2 ± 0.1
1.0	1.9	1.0	-9.6 ± 1.7	0.58	1.84	7.6 ± 0.1

TABLE IV. Thermal Diffusion data: Separate variation of every species 1 parameter at the state point $\bar{T}^* = 0.85$, $\bar{\rho}^* = 0.81$. Species 2 corresponds to Lennard-Jones Argon. The error is estimated by linear regression (in case of S_T of the temperature and mole fraction profiles). For the self diffusion coefficients, the error is generally $\pm 2\%$.

Model system	m_1/m_2	σ_1/σ_2	$\varepsilon_1/\varepsilon_2$	e_1/e_2	simulated S_T [$10^{-3} K^{-1}$]	predicted ¹ S_T [$10^{-3} K^{-1}$]	predicted ² S_T [$10^{-3} K^{-1}$]	absolute ¹ deviation [$10^{-3} K^{-1}$]	relative ¹ deviation [%]
$Ar_{\text{Iso}} - Ar$	1.50	1.00	1.00	1.00	5.0 ± 0.5	3.9	3.9	1.1	22.0
$Xe - Kr$	1.57	1.03	1.23	1.13	5.1 ± 0.7	6.2	6.3	-1.1	-21.6
$Kr - Ar$	2.1	1.07	1.39	1.13	14.4 ± 1.2	10.8	10.1	3.6	25.0
$Ar - CH_4$	2.49	0.91	0.79	1.05	9.3 ± 0.7	10.7	11.2	-1.4	-15.0
$Xe - Ar$	3.29	1.17	1.72	1.07	18.6 ± 0.8	20.4	16.0	-1.8	-9.7
$Kr - CH_4$	5.22	0.97	1.10	1.21	22.3 ± 0.6	24.3	24.8	-2.0	-9.0
$Xe - CH_4$	8.17	1.06	1.35	1.13	23.1 ± 0.7	24.5	24.1	-1.4	-6.1
$Ar_{\text{Iso}} - Ar$	8.00	1.00	1.00	1.00	24.6 ± 0.8	22.4	22.4	2.2	8.9

TABLE V. Soret coefficients for several simple atomic systems at the state point $\bar{T}^* = 0.85$, $\bar{\rho}^* = 0.81$. The run length was $4.0 \cdot 10^6$ steps. Additionally, the data for two isotopic systems is presented. A comparison indicates, that S_T is chiefly governed by the mass ratio. The error is estimated by error propagation from the errors of the slopes of temperature and mole fraction profiles as obtained in the linear regression.

¹ using Eqns. 4.1,4.2 and 4.3

² using Eqns. 4.1 and 4.4

List of Figures

1	Subdividing the periodic simulation box into slabs. Slab 0 is defined to be the cool slab, slab $N_s/2$ to be the hot slab. Kinetic energy is artificially transferred by the heat exchange algorithm and flows back by thermal conduction.	19
2	Typical profiles of system properties at the state point $\bar{T}^* = 0.81$, $\bar{\rho}^* = 0.85$. $\sigma_1/\sigma_2 = 1.2$ and species 2 corresponds to Lennard-Jones Argon. Slab 0 is defined to be the hot slab, slab 10 to be the cool slab.	19
3	Linear response regime and extrapolation to zero temperature gradient. Model system: $m_1/m_2 = 4.0$, $\sigma_1/\sigma_2 = 1.0$ and $\varepsilon_1/\varepsilon_2 = 1.3$ where species 2 corresponds to Lennard-Jones Argon. A straight line was fitted to the data points (with the highest and the lowest point omitted) in a linear scale. The extrapolation value is $S_T = 22.3 \cdot 10^{-3}/K$	20
4	(a) Soret coefficient for variations of the mass of species 1 ($m_1 > m_2$). Species 2 corresponds to Lennard-Jones Argon. (b) Self diffusion coefficients for the same systems.	21
5	(a) Soret coefficient for variations of the potential well depth of species 1. Species 2 corresponds to Lennard-Jones Argon ($\varepsilon_1 > \varepsilon_2$). (b) Self diffusion coefficients for the same systems. In spite of a stronger interaction the mobilities increase because the average temperature is raised accordingly, in order to maintain $T^* = 0.85 = \text{const}$ (Table I).	22
6	(a) Soret coefficient for variations of the diameter of species 1 ($\sigma_1 > \sigma_2$). Species 2 corresponds to Lennard-Jones Argon. (b) Self diffusion coefficients for the same systems.	23
7	Scaling behaviour of the self diffusion coefficient for diameter variations. Inset: For large diameter ratios, the slab concentration of the bigger species is nearly independent of the ratio.	24
8	The Soret coefficient varies approximately linearly with the ratio of 'cohesive energy densities' $e_1/e_2 > 1$ ($e_k = \varepsilon_k/\sigma_k^3$). Circles: The data for $e_1/e_2 < 1$ were calculated from σ_1/σ_2 variations at constant $\varepsilon_1/\varepsilon_2 = 1$. For the data at $e_1/e_2 > 1$, $\varepsilon_1/\varepsilon_2$ was varied at constant $\sigma_1/\sigma_2 = 1$. Triangles: $\varepsilon_1/\varepsilon_2$ was varied at constant $\sigma_1/\sigma_2 = 1.1$	25
9	Solid Circles: Correlation of predicted (Eqns. 4.1,4.2 and 4.3) and simulated Soret coefficients (Table V). Open Diamonds: A prediction only using Eqn. 4.1 shows that the Soret effect is dominated by the mass ratio.	26

FIGURES

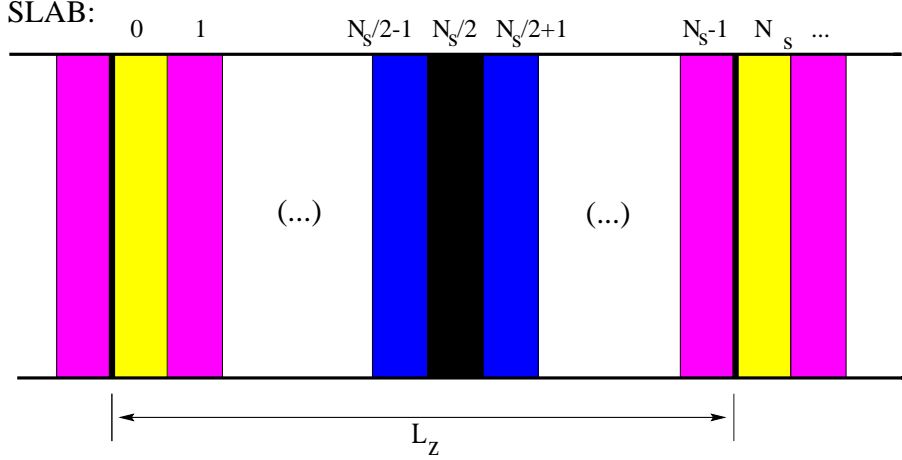


FIG. 1. Subdividing the periodic simulation box into slabs. Slab 0 is defined to be the cool slab, slab $N_s/2$ to be the hot slab. Kinetic energy is artificially transferred by the heat exchange algorithm and flows back by thermal conduction.

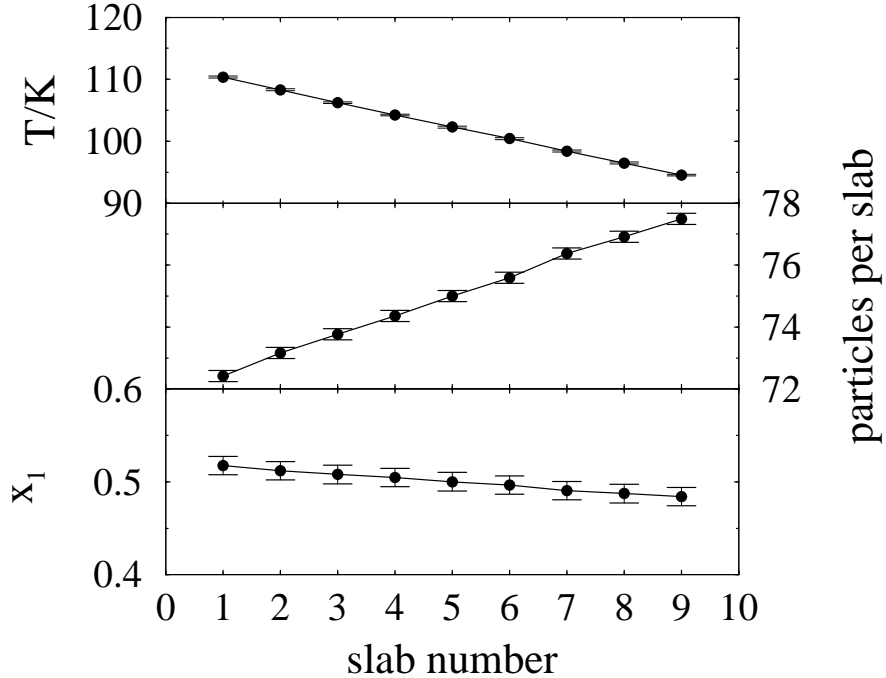


FIG. 2. Typical profiles of system properties at the state point $\bar{T}^* = 0.81$, $\bar{\rho}^* = 0.85$. $\sigma_1/\sigma_2 = 1.2$ and species 2 corresponds to Lennard-Jones Argon. Slab 0 is defined to be the hot slab, slab 10 to be the cool slab.

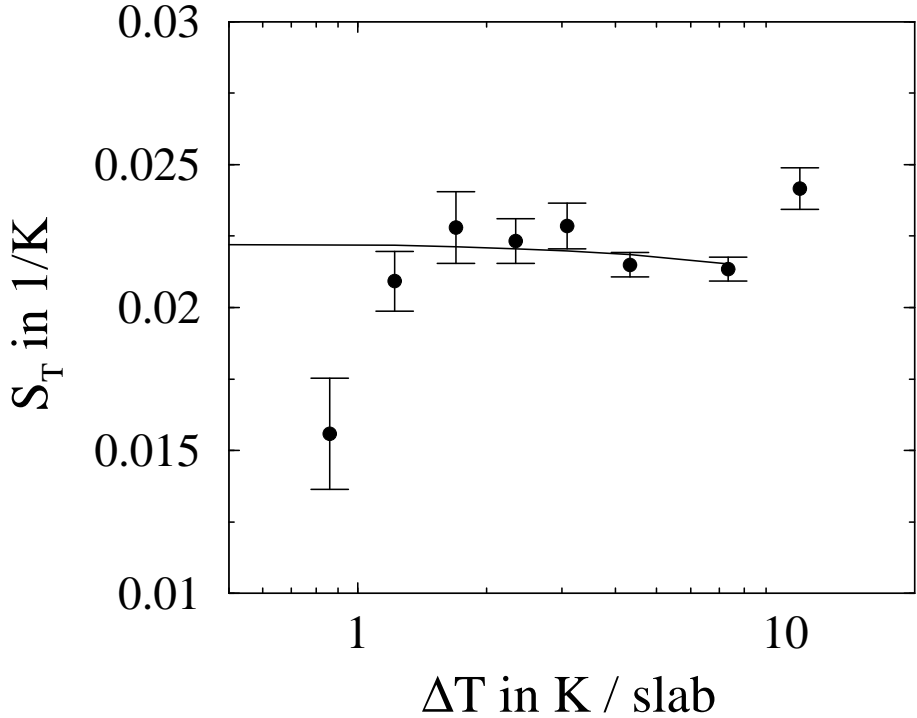


FIG. 3. Linear response regime and extrapolation to zero temperature gradient. Model system: $m_1/m_2 = 4.0$, $\sigma_1/\sigma_2 = 1.0$ and $\varepsilon_1/\varepsilon_2 = 1.3$ where species 2 corresponds to Lennard-Jones Argon. A straight line was fitted to the data points (with the highest and the lowest point omitted) in a linear scale. The extrapolation value is $S_T = 22.3 \cdot 10^{-3}/K$.

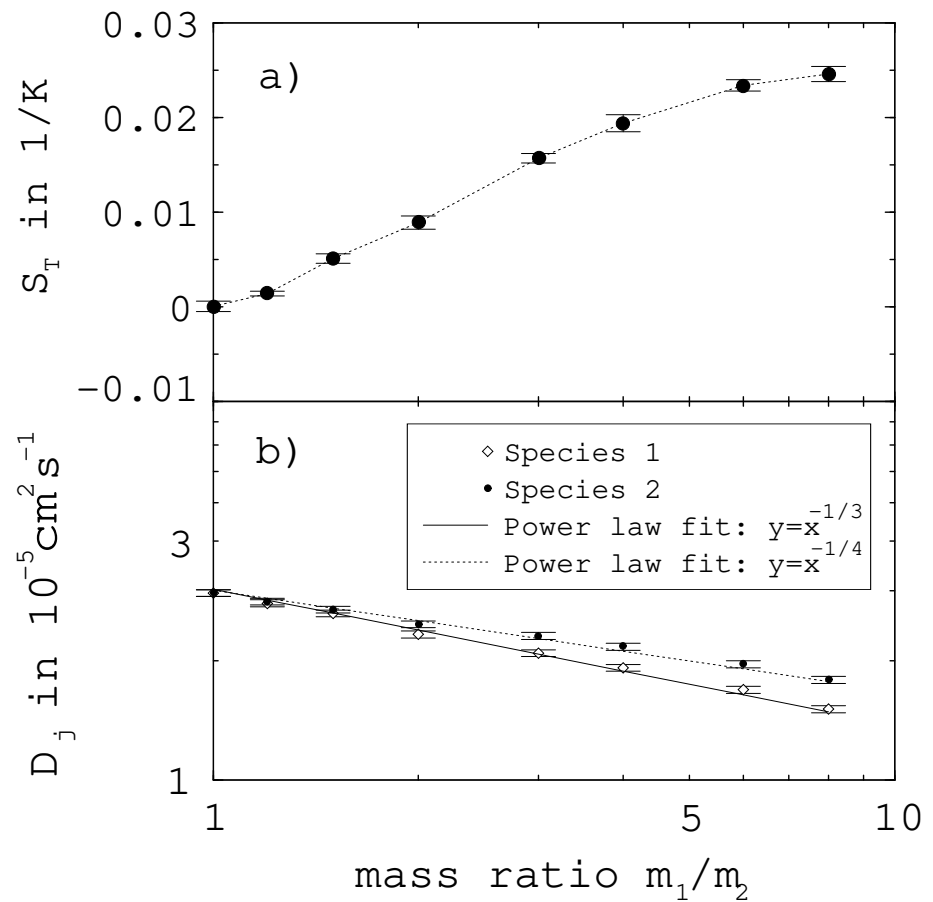


FIG. 4. (a) Soret coefficient for variations of the mass of species 1 ($m_1 > m_2$). Species 2 corresponds to Lennard-Jones Argon. (b) Self diffusion coefficients for the same systems.

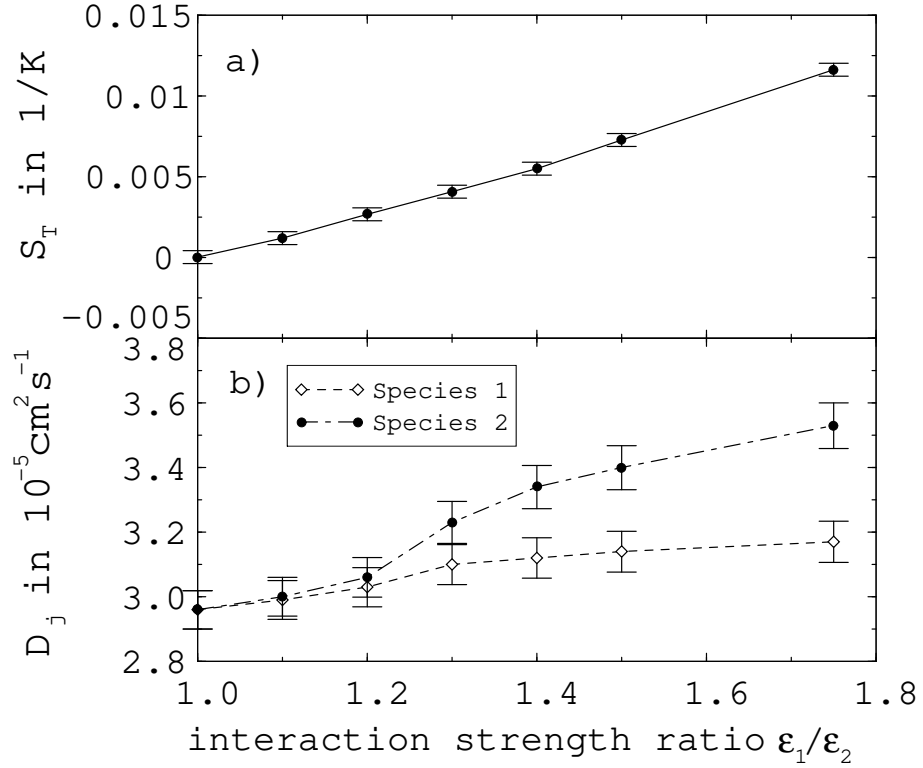


FIG. 5. (a) Soret coefficient for variations of the potential well depth of species 1. Species 2 corresponds to Lennard-Jones Argon ($\varepsilon_1 > \varepsilon_2$). (b) Self diffusion coefficients for the same systems. In spite of a stronger interaction the mobilities increase because the average temperature is raised accordingly, in order to maintain $T^* = 0.85 = \text{const}$ (Table I).

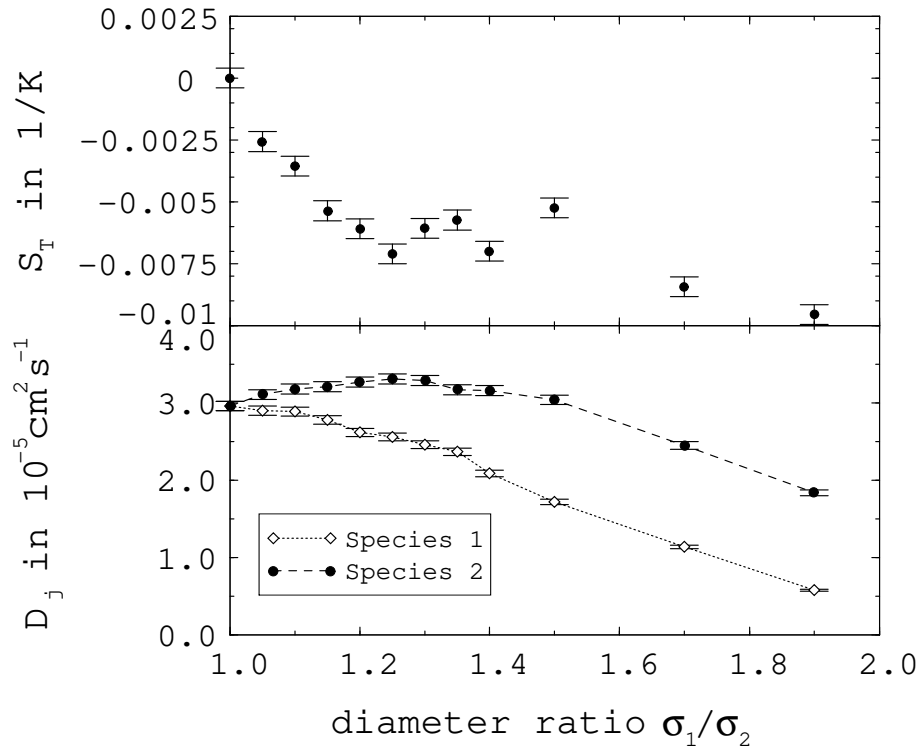


FIG. 6. (a) Soret coefficient for variations of the diameter of species 1 ($\sigma_1 > \sigma_2$). Species 2 corresponds to Lennard-Jones Argon. (b) Self diffusion coefficients for the same systems.

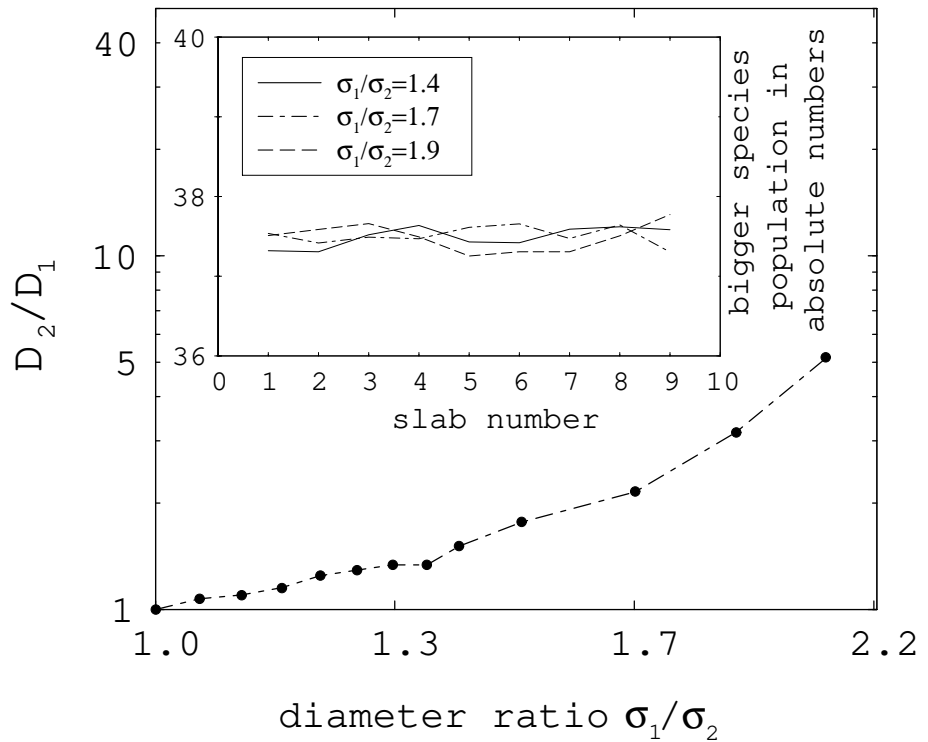


FIG. 7. Scaling behaviour of the self diffusion coefficient for diameter variations. Inset: For large diameter ratios, the slab concentration of the bigger species is nearly independent of the ratio.

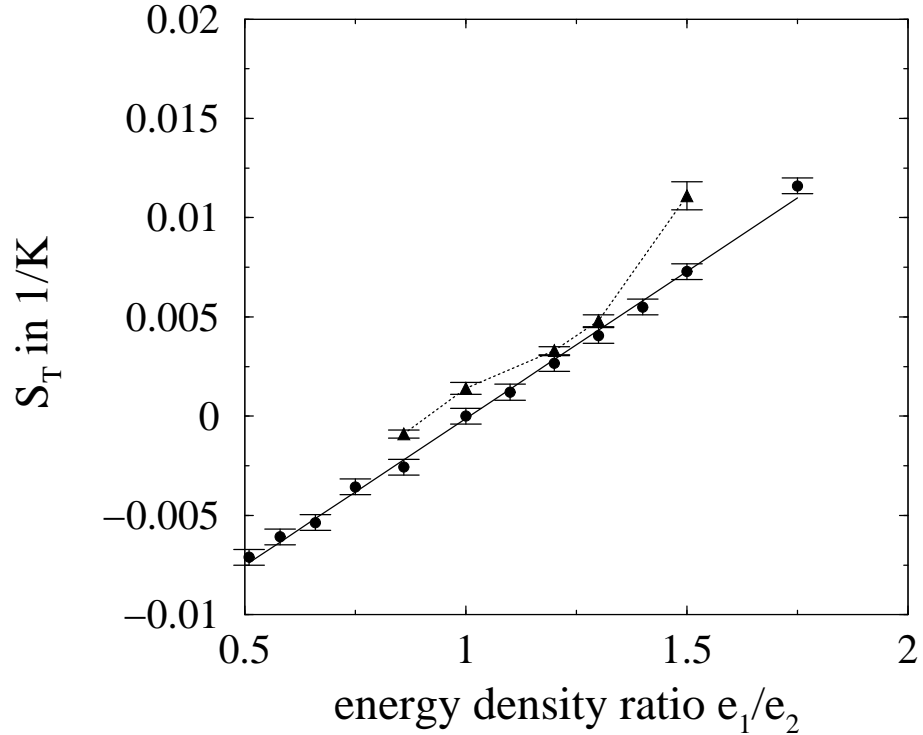


FIG. 8. The Soret coefficient varies approximately linearly with the ratio of 'cohesive energy densities' $e_1/e_2 > 1$ ($e_k = \varepsilon_k/\sigma_k^3$). Circles: The data for $e_1/e_2 < 1$ were calculated from σ_1/σ_2 variations at constant $\varepsilon_1/\varepsilon_2 = 1$. For the data at $e_1/e_2 > 1$, $\varepsilon_1/\varepsilon_2$ was varied at constant $\sigma_1/\sigma_2 = 1$. Triangles: $\varepsilon_1/\varepsilon_2$ was varied at constant $\sigma_1/\sigma_2 = 1.1$.

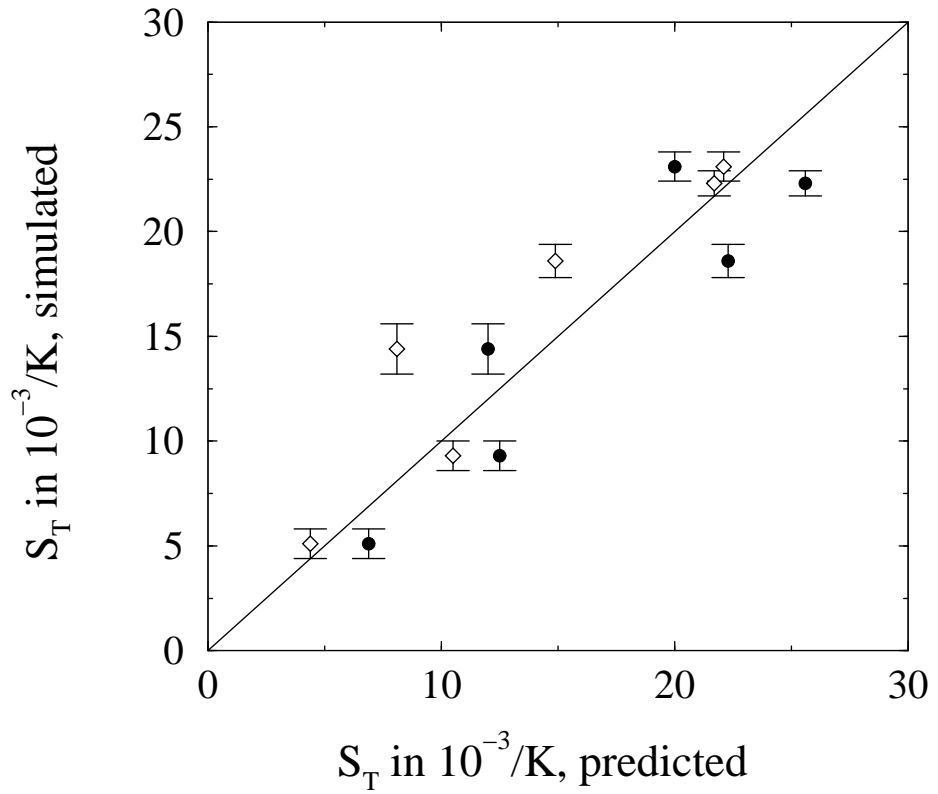


FIG. 9. Solid Circles: Correlation of predicted (Eqns. 4.1, 4.2 and 4.3) and simulated Soret coefficients (Table V). Open Diamonds: A prediction only using Eqn. 4.1 shows that the Soret effect is dominated by the mass ratio.

REFERENCES

- ¹ C. LUDWIG, *Sitz.ber. Akad. Wiss. Wien Math.-naturw. Kl.* **20**, 539 (1856).
- ² C. SORET, *Arch. Geneve* **3**, 48 (1879).
- ³ D. ENSKOG, *Ann.Phys.* **36**, 731 (1912).
- ⁴ S. CHAPMAN, *Philos.Trans.Ser.A* **217**, 115 (1917).
- ⁵ S. CHAPMAN and F. DOOTSON, *Philos.Mag.* **33**, 248 (1917).
- ⁶ K. CLUSIUS and G. DICKEL, *Naturwissenschaften* **26**, 546 (1938).
- ⁷ J. C. GIDDINGS, K. D. CALDWELL, and M. N. MYERS, *Macromolecules* **9**, 106 (1976).
- ⁸ W. KÖHLER and P. ROSSMANITH, *Int.J.Polymer Analysis and Characterization* **1**, 49 (1995).
- ⁹ J. KINCAID and B. HAFSKJØLD, *Mol.Phys.* **82**, 1099 (1994).
- ¹⁰ B. HAFSKJØLD and S. RATKJE, Coupled Transport of Heat and Mass. Theory and Applications, in *Entropy and Entropy Generation*, edited by J.S.SHINER, pp. 197–219, Kluwer Academic Publishers, Dordrecht, 1996.
- ¹¹ J. D'ANS and E. LAX, editors, *Taschenbuch für Chemiker und Physiker, Band1*, Springer, Berlin, 1992.
- ¹² L. ONSAGER, *Phys.Rev.* **37**, 405 (1931).
- ¹³ D. MACGOWAN and D. EVANS, *Phys.Rev.A* **34**, 2133 (1986).
- ¹⁴ D. MACGOWAN, *Phys.Rev.A* **36**, 1367 (1987).
- ¹⁵ G. PAOLINI and G. CICCOTTI, *Phys.Rev.A* **35**, 5156 (1987).
- ¹⁶ R. VOGELSANG and C. HOHEISEL, *Phys.Rev.A* **38**, 6296 (1988).
- ¹⁷ D. EVANS and D. MACGOWAN, *Phys.Rev.A* **36**, 948 (1987).
- ¹⁸ B. HAFSKJØLD and T. IKESHOJI, *Mol.Phys.* **81**, 251 (1994).
- ¹⁹ B. HAFSKJØLD and T. IKESHOJI, *Molec.Sim.* **16**, 139 (1996).
- ²⁰ B. HAFSKJØLD and I. WOLD, *Int. J. Thermophys.* **20**, 847 (1999).
- ²¹ D. EVANS and G. MORRISS, *Statistical mechanics of non-equilibrium liquids*, Academic Press, New York, 1990.
- ²² D. REITH, Thermal Diffusion in binary Lennard-Jones liquids, Diploma thesis, University of Mainz, 1998.
- ²³ B. HAFSKJØLD, T. IKESHOJI, and S. RATKJE, *Mol.Phys.* **80**, 1389 (1993).
- ²⁴ F. MÜLLER-PLATHE and D. REITH, *Comp. Theor. Polym. Sci.* **9**, 203 (1999).
- ²⁵ M. ALLEN and D. TILDESLEY, *Computer Simulation of Liquids*, Oxford Science, Oxford, 1987.
- ²⁶ H. BERENDSEN, J. POSTMA, W. VAN GUNSTEREN, A. DI NOLA, and J. HAAK, *J.Chem.Phys.* **81**, 3684 (1984).
- ²⁷ M. TUCKERMAN, B. BERNE, and G. MARTYNA, *J.Chem.Phys.* **94**, 6811 (1991).
- ²⁸ F. MÜLLER-PLATHE, *J.Chem.Phys.* **106**, 6082 (1997).
- ²⁹ F. MÜLLER-PLATHE, *Phys.Rev.E* **59**, 4894 (1999).
- ³⁰ R. BEARMAN and D. JOLLY, *Molec.Phys.* **44**, 665 (1981).
- ³¹ C. HOHEISEL and R. VOGELSANG, *Comput.Phys.Rep.* **8**, 1 (1988).
- ³² R. VOGELSANG, C. HOHEISEL, G. PAOLINI, and G. CICCOTTI, *Phys.Rev.A* **36**, 3964 (1987).
- ³³ M. SCHÖN and C. HOHEISEL, *Molec.Phys.* **52**, 1029 (1984).